ORIGINAL PAPER

Morphological Factors Involved in Adhesion of Acid-Cleaned Diatom Silica

**Katarzyna S. Kopanska · Benoit Tesson · Haisheng Lin ·
J. Carson Meredith · Mark Hildebrand · Aubrey Davis**

Abstract

Purpose Diatoms, unicellular microalgae with silica cell walls, have strong adhesive properties, which are dominated by chemical interactions between secreted organic material and the substrate. Possible technological applications of diatoms are likely to involve the adhesion of silica particles, or derivatives, which have been cleaned of organic material. Because the morphologies of diatom cell walls are far more complex than defined model structures, the relationship between morphology and adhesion for such materials is unknown.

Methods In this paper we develop a new approach to monitor the adhesion of acid-cleaned diatom silica using parallel-plate flow chambers. We have evaluated factors such as settling time, extent of dryness, and substrate properties, and compared diatom species with silica features differing in size, shape, and percentage of surface contact area.

Results Results indicated better adhesion of particles with higher surface contact area below a threshold of overall size, and a contribution by the number of possible contact surfaces to initial adhesion. We identified two stages in adhesion response to increasing shear stress. In the first stage, at low shear stress, species-dependent morphology played a major role in determining the strength of adhesion. After loosely adhered particles were removed at low shear, a second stage of persistent adhesion emerged at higher shear stresses. In the second stage, variations in morphology had a much smaller effect on adhesion.

Conclusions These results identify conditions and fundamental morphological features for adhesion that can be utilized in future technological applications of silica particles with complex shapes.

Keywords Diatoms · Adhesion · Silica · Morphology

K. S. Kopanska · B. Tesson · M. Hildebrand · A. Davis (✉)
Marine Biology Research Division,
Scripps Institution of Oceanography, University of California San Diego, 9500 Gilman Dr., La Jolla, CA 92093-0202, USA
e-mail: akdavis@ucsd.edu

H. Lin · J. C. Meredith
School of Chemical and Biomolecular Engineering,
Georgia Institute of Technology, 311 Ferst Drive NW,
Atlanta, GA 30332-0100, USA

Present Address:
K. S. Kopanska
Laboratoire PhysicoChimie, UMR168, Institut Curie,
11 rue Pierre et Marie Curie, 75005 Paris, France
e-mail: katarzyna.kopanska@cantab.net

1 Introduction

Diatoms, a type of microscopic algae with silica cell walls, are known for their strong adhesion to natural and man-made surfaces. The adhesive properties of these organisms are contributing factors to their evolutionary success and ubiquitous distribution in aquatic environments [1]. Adhesion of living diatom cells is dominated by chemical interaction with the substratum [1, 2] *via* secreted extracellular mucilage. The chemically driven mechanisms of living diatom adhesion have been studied and are at least partially understood [2–7].

Diatom cell wall silica consists of essentially pure SiO_2, with a small contribution of organic material involved in its formation and associated with its surface. Acid-cleaning diatom silica removes all surface-associated organic

material [8]. Enzymatically-cleaned diatom silica has surface characteristics similar to Aerosil 200 [9]. Diatom silica has potential applications in materials science and nanotechnology, especially considering the unique and varied structures [10–15]. The material is characterized by unique optical properties [16–18] and can be converted by a variety of means into other functional chemistries [19, 20]. It is estimated that there are more than 2×10^5 different diatom species, each with distinct silica features, which vary on nanometer to micron scales [21–23]. The silica cell wall (called the frustule) is divided into two parts with overlapping halves consisting of a valve, characterized by a variety of adornments, and girdle bands, that are commonly unornamented silica strips that hold the halves together [24]. Diatoms occur in two general structural classes based on valve shape, with the centric class exhibiting radial symmetry and the pennate class exhibiting bilateral symmetry [25]. The raphe is a predominant characteristic of raphid pennate diatoms and provides the predominant contact surface in living cells with the substrate either along the center of the valve or on one side [25].

Practical technological applications of diatom silica will likely involve assembly at larger scales on surfaces. For example, diatom-derived silica particles could be used as taggants, tailored to attach to particular surfaces. In contrast to the effort devoted to understanding adhesion of living diatoms, the adhesion of acid-cleaned diatom silica to surfaces has not been studied. Well-defined synthetically made shapes of silica have been investigated in this regard, and results indicate that a variety of mechanisms may be involved in their adhesion [26]. Due to the diversity of sizes, shapes and mesoscale morphology of diatom silica, straightforward extrapolation of results from studies of synthetic model silica particles, usually spheres, is not likely to be valid. Native diatom silica needs to be directly evaluated to understand the factors involved in its adhesion.

Previously, adhesion assays were conducted on living biofouling diatoms in large, turbulent flow channels in which upwards of 80 liters of media was circulated [6]. These systems were not designed for real-time imaging of cells subjected to shear stress; consequently, the substratum had to be removed and examined after each flow rate was applied. Hodson et al. (2012) recently developed a turbulent flow channel that does allow real-time imaging of living cells, however, the resolution is not adequate for imaging of acid-cleaned silica material and small diatom species [27]. These constraints highlight the need for a chamber that couples appropriate shear force capabilities with compact size, which would permit high-resolution, real-time imaging of the adhesive characteristics of silica material with a standard microscope.

In this study we adapt parallel-plate flow chambers (PFCs) to develop a new approach to monitor adhesion of acid-cleaned diatom silica. We explore how morphological factors such as size, geometry and mesoscale structure contribute to adhesion of diatom silica. We identify fundamental factors involved in adhesion that can be utilized in technological applications of diatom silica particles.

2 Material and Methods

2.1 Diatom Culture Conditions and Silica Preparation

Navicula pelliculosa FW was grown in fresh water tryptone medium [28] and other diatom species in artificial seawater medium [29] supplemented with biotin and vitamin B12, each at 1 ng L^{-1}, or artificial seawater medium according to the North East Pacific Culture Collection protocol (http://www3.botany.ubc.ca/). Growth was performed at 18–22°C in continuous light (150 μmol m^{-2} s^{-1}). Diatom silica was cleaned by sulfuric acid treatment as described elsewhere [30].

2.2 Silica Characterization by Scanning Electron Microscopy and Atomic Force Microscopy

Scanning electron micrographs were acquired with an FEI SFEG UHR (FEI Company, Hillsboro, OR, USA) Scanning Electron Microscope at the University of California San Diego Nano3 Facility on samples that had been sputter coated with iridium.

Atomic force microscopy was performed in air on frustules that had been dried on poly-L-lysine coated slides. Images were acquired in ScanAsyst mode using a silicon cantilever with a spring constant of 5 N/m (TAP150, Bruker) on a Veeco Bioscope Catalyst Atomic Force Microscope coupled with a Zeiss inverted fluorescent microscope. AFM images were processed using WSxM 4.0 software [31] and Nanoscope analysis 1.40.

2.3 Parallel-Plate Flow Chamber (PFC) Method

Figure S1 presents the scheme of the experimental setup used in the study. Microchambers for cell settling were fabricated by cutting off the top 1.5 cm of a 17 mm diameter plastic test tube (VWR International, Radnor, PA, USA), placing the uncut opening against the glass microscopy slide and securing it with binder clamps. To prevent slides from breaking due to uneven pressure, two additional slides were clamped underneath for added support. A solution of silica particles in deionized water at near neutral pH was

pipetted into the microchambers and settled overnight (at least 16 h) at 18 °C to minimize water evaporation. The ProFlow chamber (PFC-1) from Warner Instruments (Hamden, CT, USA) was assembled as described by the manufacturer with one exception; the 25 mm round cover glass forming the bottom of the chamber was replaced by a standard glass slide (75 × 25 × 1 mm) onto which the diatom silica was allowed to settle. The assembled chamber was mounted on a Zeiss AxioObserver inverted microscope (Carl Zeiss Microimaging, Inc., Thornwood, NY, USA).

An image was taken immediately (Control 1) to demonstrate saturation of the surface with silica particles. Low flow was then applied (0.75 Pa shear stress) to gently remove unattached cells and another image was taken (Control 2) to show initial adhesion. Subsequently, the flow rate was increased in a step-wise manner from 10 to 155 mL/min with a PHD Ultra syringe pump (Harvard Apparatus, Holliston, MA, USA) resulting in incremental increases in shear stress (1.5–24 Pa). Based on the Navier-Stokes equations applied to the dimensions of the PFC-1 chamber for water, each 1 ml/min of flow rate yields 0.15 Pa shear stress on the chamber walls. When used in conjunction with the PHD Ultra syringe pump, which has a maximum flow rate of 220 mL/min, shear stresses in excess of 30 Pa could be achieved. Even at this high flow rate, the Reynolds number is ∼700, which is well within the laminar flow regime. Images were taken after each flow rate increment to examine particle retention on the slide. Cell numbers were counted using ImageJ software (National Institutes of Health, USA). Only valves and not girdle bands were taken into account when assessing the number of adhered particles.

2.4 Hydrophobic Self-assembled Monolayer (SAM) Slides

The two alkanethiols, 1-dodecanethiol (CH$_3$-thiol, [CH$_3$(CH$_2$)$_{11}$SH], ≥98 %, Sigma-Aldrich) and 11-mercapto-1-undecanol (OH-thiol, [HO(CH$_2$)$_{11}$SH], 97 %, Sigma-Aldrich), were used as received without further purification. Absolute ethanol (VWR Scientific) was used as a solvent. The substrates for self-assembled monolayer (SAM) films were prepared on standard glass microscope slides (VWR Scientific) coated by a mixture of CH$_3$-thiol and OH-thiol, a well-characterized procedure for surface functionalization described previously [32]. The glass slides were first cleaned with *piranha* solution (30:70 volume of 30 wt % H$_2$O$_2$ and concentrated H$_2$SO$_4$(95–98 %)) at 80 °C for 2 h to remove any trace organics, and then thoroughly rinsed in deionized H$_2$O, and dried with nitrogen gas. The glass substrates were then coated with a 60 nm gold film in a gold sputtering system.

Stock solutions were prepared by dissolving CH$_3$-thiol, or OH-thiol, or a mixture of both thiols in ethanol at an overall concentration of 1 mM. The gold coated glass substrates were then immersed in the thiol solutions overnight at 4 °C. The SAMs remained in the thiol solutions at 4 °C until they were used, at which time they were rinsed in ethanol and dried under a stream of nitrogen gas. A series of SAMs with variation in surface wettability was prepared with mixed thiol solutions having different molar percentages of CH$_3$- and OH-thiols (0/100, 20/80, 40/60, 100/0).

Static water contact angles were measured on the different SAM glass substrates using a video contact angle 2500XE system (AST products, Billerica, MA). Nine 1 μl drops were dispensed onto the sample surfaces. Both the right and left angles between the sample surface and the tangent line to each droplet were measured. The calculated contact angles were 22 ± 4°, 45 ± 4°, 73 ± 5°, and 108 ± 5° for SAM substrates prepared in thiol solutions with CH3/OH thiol molar percentages of 0/100, 20/80, 40/60, and 100/0, respectively.

2.5 Silica Staining Using APS-FITC

In some cases, after collecting fractions of material removed from the substrate by increasing shear stress, silica was stained with APS-FITC to help with visualization during subsequent analysis involving flow cytometry and fluorescence microscopy. Silica was stained using (3-amino-propyl)trimethoxysilane - fluorescein- 5-isothiocyanate (APS-FITC) based on methods described by Blaaderen & Vrij (1992) for silica particles [33] and by Descles et al. (2008) for diatom silica [34].

2.6 Imaging Flow Cytometry Analysis

Eluents of *A. coffeaeformis* silica from the PFC experiment were collected, concentrated by centrifugation, and stained using the APS-FITC method. Particle separation and imaging was performed on an imaging flow cytometer (ImageStream X, Amis Corporation, Seattle, USA). Images of five thousand particles were acquired for each sample. The data were analyzed using software (IDEAS, Amis Corporation) provided by the manufacturer.

2.7 Zeta Potential Measurements

Zeta potentials were measured by electrophoresis (Malvern Zetasizer Nano ZS-90) in a 1 mM NaCl background electrolyte on a sample of *A. coffeaeformis* acid-cleaned silica. The zeta potential was evaluated from the measured electrophoretic mobility by using the Smoluchowski

approximation for large ratios of particle radius to Debye screening length.

3 Results

3.1 Development of the Parallel-Plate Flow Chamber for Adhesion Measurements

Parallel-plate flow chambers have been used to monitor cell behavior under blood flow pressure regimes, which are typically up to 3 Pa [35, 36]. We desired to investigate diatom silica adhesion at shear stresses up to 30 Pa an upper limit to which diatoms are exposed in the natural environment, which necessitated adaptation of commercially available PFC units. Two general designs were commercially available. The first design relied on vacuum to maintain a seal that held the chamber together. This seal failed when exposed to high flow rates (data not shown). In the second design (Warner Instruments PFC-1), the chamber was held together securely by screws and could withstand high flow rates without being compromised. In the standard commercial system the chamber was created between a 15 mm and a 25 mm round coverglass. It was determined that the 25 mm coverglass was too flexible, resulting in image distortion and eventual failure. The PFC-1 design permitted replacement of the 25 mm coverglass with a standard 1 mm thick glass slide, providing the necessary stiffness and strength for imaging capability. A method was developed to minimize the volume of material required for uniform settling on the slides using settling chambers (see Section 2.3 and Fig. S1). These modifications enabled determination of the adhesive properties of diatom silica particles with minimal sample requirement.

The methodology for monitoring adhesion involved settling a saturating amount of cleaned silica from each species on a glass slide overnight, then gently removing the non-adherent particles at low shear stress (0.75 Pa). The particles remaining after this treatment represent the initial adhesion. Examples of the number of particles applied, and those remaining after the low pressure treatment are shown in Fig. 1. Control experiments showed that the number of particles applied on the slide above a saturating level had no effect on the number of cells initially adhering (Fig. S2).

3.2 Factors Influencing Particle Adhesion

To understand how various factors might affect the adhesion of silica such as the effect of drying, settling time and substrate properties, we performed a series of experiments with silica from *Amphora coffeaeformis*. This species

was chosen because initial experiments demonstrated that it was particularly adhesive. At pH = 7 acid-cleaned *A. coffeaeformis* diatom silica particles had a zeta potential of −24.7 Å ± 0.5 mV, which is similar to values reported for similarly-sized commercial silica spheres [37].

3.2.1 Effect of Drying

The initial adhesion of *A. coffeaeformis* silica applied to a slide in water was compared to that in which water was allowed to evaporate to dryness at room temperature. Figure 2 shows that initial adhesion (after washing at 0.75 Pa) and adhesion during increasing pressure (18 Pa) was higher when particles were dried on the slide compared with those maintained in water. It also shows extensive aggregation of particles after drying as compared to the wet sample. Subsequent experiments were conducted exclusively with wet samples because aggregation that occurred in the dried samples would complicate the evaluation of the adhesion of diatom silica to the substrate, and dried material adhered to such an extent that meaningful measurements of adhesive properties at various pressures were not possible.

3.2.2 Initial Adhesion and the Effect of Settling Time

To evaluate the effect of settling time on initial adherence and to determine the time to achieve the highest number of adherents, a settling time course experiment was performed using *A. coffeaeformis*. Equivalent numbers of particles were allowed to settle from 30 min to 24 hours and then subjected to a shear stress of 0.75 Pa. Figure 3 shows that the number of adhered particles increased until 16 hours and then plateaued. Therefore we concluded that a settling time of at least 16 hours was sufficient to achieve a maximum number of adhered particles.

3.2.3 Substrate Properties

The adhesion of silica particles from *A. coffeaeformis* to substrates with different hydrophobic properties was investigated by comparing adhesion to glass slides with slides coated with a self-assembled monolayer (SAM) ranging in hydrophobicity from low, contact angle (CA) 25°, to high, CA 75°. The initial retention of particles was highest on the hydrophilic glass surface and decreased with increasing hydrophobicity (Fig. 4a). By plotting the percentage of particles adhering relative to initial adhesion, the behavior of initially adhered particles was monitored. The data in Fig. 4b show that once attached, the particles behaved in a similar fashion.

Fig. 1 Initial adhesion of silica from a pennate (*A. coffeaeformis*) and centric (*C. cryptica*) diatom species. *Left panels* show the amount of diatom silica settled on the glass slides. *Right panels* show the same slides after the application of a low shear stress (0.75 Pa) representing the initial number of adherent silica particles
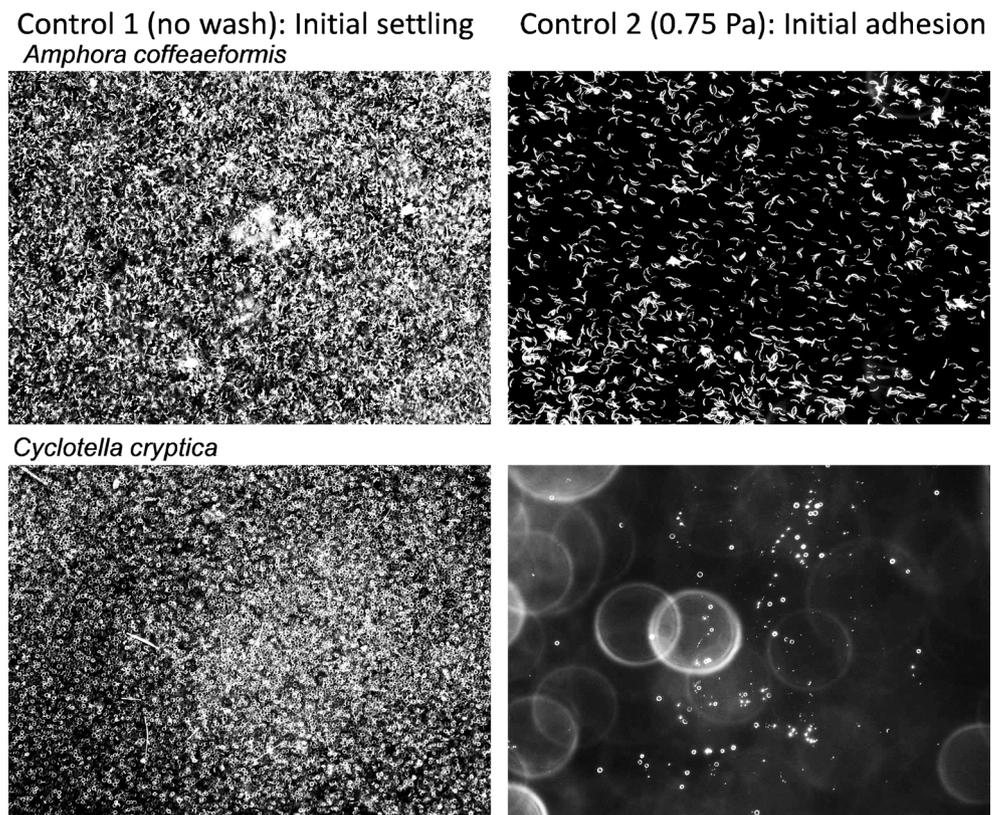
3.3 Comparison of the Adhesion to Glass Slides of Silica from Six Species

Six diatom species displaying different shape, size and mesoscale features were selected for adhesion experiments on glass with the PFC (Fig. 5a). The three centric diatoms had circular valves that ranged in diameter from 4 μm (*Thalassiosira pseudonana*), to 7 μm (*Thalassiosira oceanica*) to 9 μm (*Cyclotella cryptica*), and in complexity in surface texture from *T. oceanica* (smooth surface), to *C. cryptica* (scalloped surface), to *T. pseudonana* (complex ridged surface). The pennate species ranged in size from 3 × 5 μm (*Navicula pelliculosa*), to 16 × 3 μm (*Amphora coffeaeformis*) to 35 × 5 μm (*Craspedostauros australis*). *N. pelliculosa* and *C. australis* had oval or elongated oval shapes, whereas *A. coffeaeformis* had a more complex, banana-like shape (Fig. 5a). *N. pelliculosa* had a relatively smooth surface, *A. coffeaeformis* also had a smooth surface with pores present, and *C. australis* had a moderately ridged surface.

Adhesion of cleaned silica from different species was compared (Fig. 5b, c). In terms of initial adhesion, the rankings from lowest to highest were *C. australis*, *T. oceanica*, *C. cryptica*, *T. pseudonana*, *N. pelliculosa*, and *A. coffeaeformis* (Fig. 5b). For centric diatoms the trend was generally consistent with the expected extent of surface contact,

addressed observationally here, and in more experimental detail later (see Section 3.4).

Plotting the percent retention after 0.75 Pa demonstrates persistence in adhesion once adhered. As can be seen (Fig. 5c), the removal patterns tend to follow a generally linear trend. There are two possible exceptions, with *T. pseudonana* and *A. coffeaeformis*. *T. pseudonana* may be more sensitive to removal between 1.5 and 3 Pa than other species, and *A. coffeaeformis* appears to adhere more effectively than other species between 6 and 18 Pa (Fig. 5c). Comparing the shear stress at which 50 % of particles are removed, the most persistent particles were *A. coffeaeformis* (18 Pa), followed by *C. australis* and *T. oceanica* (12 Pa), *C. cryptica* and *N. pelliculosa* (6 Pa) and *T. pseudonana* (3 Pa).

3.4 Contact Area and Mesoscale Features

The species comparison experiment (Fig. 5) suggested that a possible determinant of initial adhesion was the mesoscale silica morphology that dictated the area of contact between the particles and the substrate.

To address possible differences in surface contact area, two species with closely related shapes but different mesoscale structures, *T. oceanica* and *T. pseudonana* were investigated using SEM and AFM imaging (Fig. 6a). The

Fig. 2 Comparison of the adhesion of *A. coffeaeformis* silica particles applied to glass slides and either dried or maintained wet. *Top panels* show initial adhesion of particles after the application of a low shear stress (0.75 Pa) and *bottom panels* show the same area after subjecting particles to 18 Pa shear stress
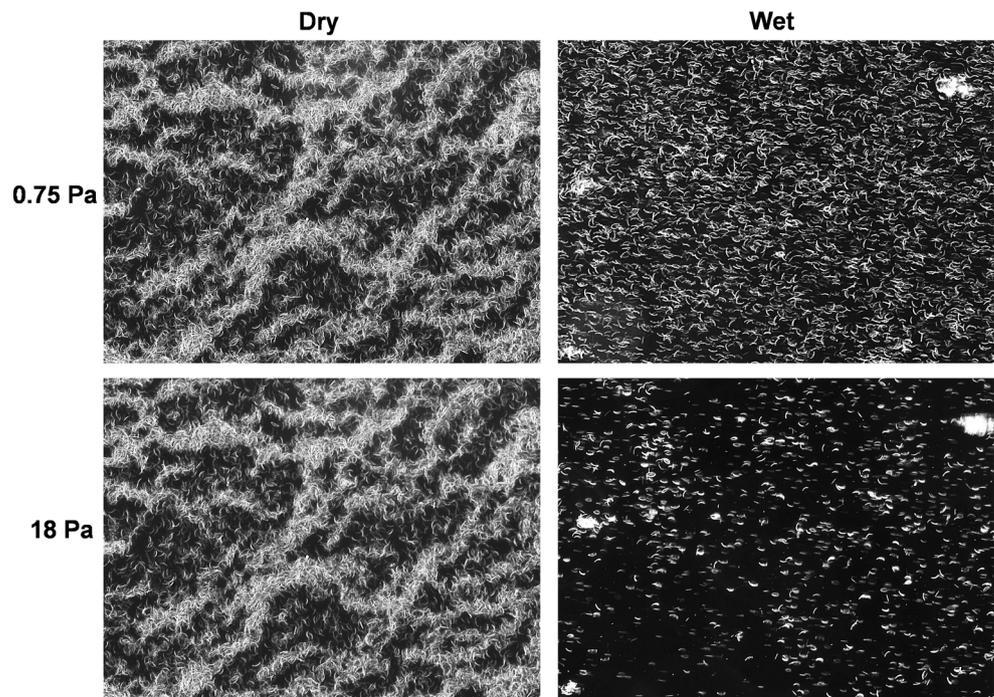
rims of the valves in both species are similar, but the valves have significantly different internal morphology. The valve of *T. oceanica* is characterized by smooth texture with small pores (Fig. 6a i, ii) while *T. pseudonana* valves are ornamented on the surface with raised silica ribs radiating from the center (Fig. 6a vi, vii). It is widely accepted that for a mesostructured particle, contact with a flat surface will occur on the outermost ornamentation [38]. Analysis of the AFM results indicates that *T. pseudonana* has far larger surface area available for contact relative to the overall external surface area than *T. oceanica*, whose contact points are only around the edges and a small area in the center (Fig. 6a iii and viii, respectively). We also performed profile measurements that confirmed *T. oceanica* has contact points on the edges and the middle pore, whereas *T. pseudonana* has more extensive potential contact surfaces covering the entire valve (Fig. 6a iv, v and ix, x, respectively).

Similar to *T. pseudonana, N. pelliculosa* is characterized by a flat valve with high percentage contact area (Fig. 6b viii, ix, x). *A. coffeaeformis* is characterized by a three dimensional shape with curved surfaces which is substantially different from the other investigated particles (Fig. 6b i and ii). AFM measurements indicate that *A. coffeaeformis* has a lower proportion of available contact surface, due to the curved nature of the valve (Fig. 6b iii and iv). In spite of this, it adhered better than *N. pelliculosa* (Fig. 5).

We examined the effects of settled valve orientation of *A. coffeaeformis* on persistent adhesion to the glass slide using SEM. The results indicate that during initial adhesion

the orientation of the valves was random with both the outside and inside of the valves in contact with the substrate (Fig. S3c, d). However after the application of shear force (Fig. S3c, d), particles adhered to the glass with the outside of the valve (higher contact area) were more persistent and remained adhered to the substrate.

3.5 Size Contribution to Adhesion

Cross-species comparison of the effect of size on adhesion is complicated due to the differences in shape and mesoscale surface features that affect adhesion, as shown above. Therefore to evaluate strictly how size contributes to adhesion, we compared adhesion of different particles derived from a single species, *A. coffeaeformis,* using imaging flow cytometry as an analysis tool. The large number of particles evaluated enabled a rigorous statistical evaluation of even small differences in size that is not possible with other approaches.

A. coffeaeformis silica was subjected to a PFC experiment in which eluate was collected during exposure to various shear forces, the silica was stained with APS-FITC and then analyzed by imaging flow cytometry. Figure 7 shows how the distribution of length and width (these were the most sensitive parameters to define dimensional differences) of silica particles changed from the control to eluted samples. In terms of length, the control sample silica showed a bell-shape distribution (mean = 14.31 μm). The length of valves in the eluted sample increased at 24 Pa
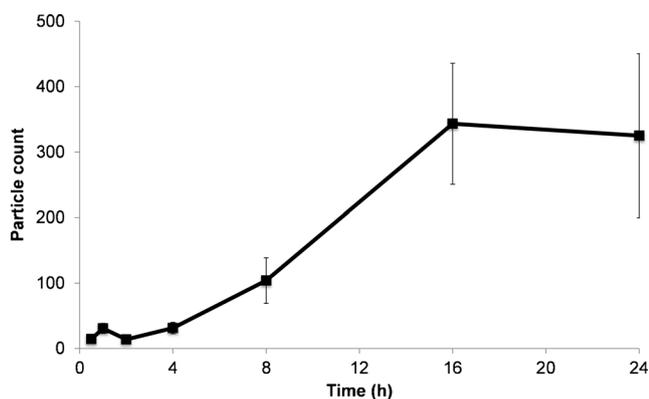
Fig. 3 Adhesion of *A. coffeaeformis* silica particles as a function of settling time shown as the number of particles remaining on the slide after exposure to 0.75 Pa. The data are mean ± SD of three independent experiments

the mean length was 15.67 μm. In terms of the distribution of silica particle widths, there was a general trend of removing narrower particles (mean = 4.95 μm at control) earlier than wider particles (mean = 5.58 μm at 24 Pa). These results suggest that at a certain shear force threshold particles with the largest contact area, defined by length and width, demonstrate increased persistent adhesion.

4 Discussion

The adhesion and detachment of synthetic silica particles to and from solid surfaces has been described [26, 37], however most studies utilized silica particles with a spherical geometry. The close agreement in zeta potential between commercial silica spheres and diatom silica used herein (at pH = 7) is expected based on the equivalence in their chemical composition. Hence, differences in adhesion between synthetic spheres reported in the literature and diatom silica in these experiments are likely due to particle shape and surface morphology. The shear forces required to detach synthetic 10 μm glass spheres from glass substrates are significantly lower (0.4 Pa at 10 % detachment) [37] than those required to detach similarly-sized diatom silica particles (1.5 to 3 Pa) (Fig. 5) under similar laminar flow conditions (Reynolds number based on particle diameter were less than 10 in both studies). Many factors are known to affect particle-substrate association in water including, size, shape, elasticity and agglomeration characteristics of the particle, and the wettability, roughness and chemistry of the particle and substrate [26]. A general conclusion is that for the same particle chemistry, smooth spherical particles make contact over a single, small contact area that is significantly smaller than the particle diameter. A complex particle such as a diatom would be expected to have multiple contact
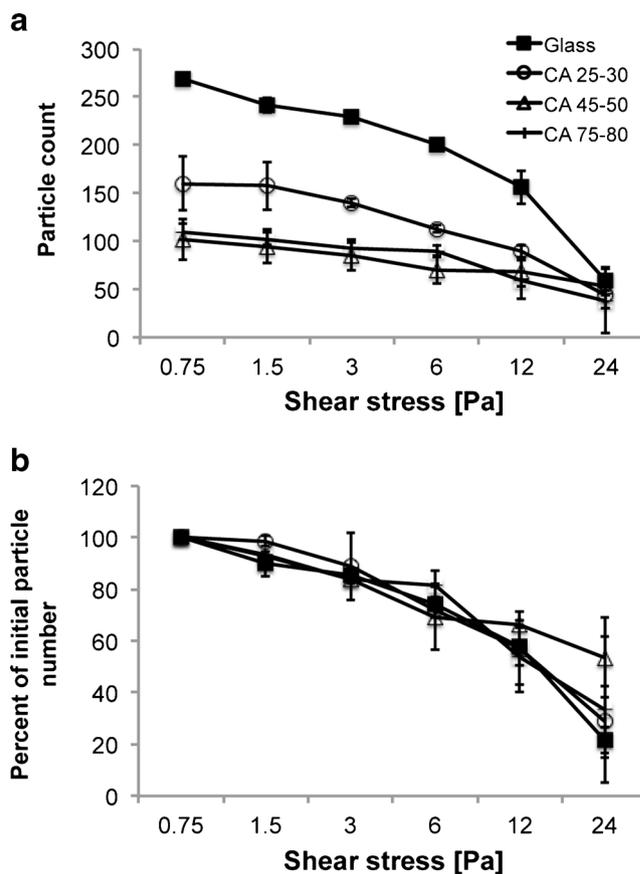
Fig. 4 Adhesion of *A. coffeaeformis* silica particles on substrates of varying hydrophobicity after incremental increases in shear stress shown as: **a** number of particles remaining on the slide after each pressure applied; **b** percentage of initially adhered particles. CA - contact angle. The data are mean ± SE of three independent experiments

points, which could encompass the majority of the surface area (Fig. 6)

A series of control experiments established that the behavior of diatom cell wall silica in the PFC corresponded with established adhesion theory. Dried *A. coffeaeformis* silica particles adhered better (Fig. 2), which is consistent with previous studies on synthetic silica [26, 39, 40]. The difference in adhesion between dry and wet particles is the result of different forces operating as particles settle and rearrange on the surface in each environment [40]. In an aqueous environment, particle-surface and particle-particle attraction will be driven by van der Waals (VDW) forces between the solids, hydration (water-surface hydrogen bonding for example), and hydrogen bonding between surface silanol groups on the frustules and the substrate. At pH = 7, a condition of this study, both diatom silica particles (measured zeta potential −24.7 Å ± 0.5 mV) and glass (−110 mV) [41] have negative charges which is expected to lead to double-layer repulsion between the particles and the surface, as well as between the particles themselves [26,

a

b

Standard error (% of the mean)						
Shear stress [Pa]	Tp	To	Cc	Np	Ac	Ca
0.75	28	14	11	14	21	9
1.5	15	8	8	8	8	8
3	22	3	8	20	2	5
6	31	9	11	18	13	12
12	37	22	18	14	23	32
18	37	39	32	30	27	33
24	38	45	40	46	40	54

c

Standard error (% of the mean)						
Shear stress[Pa]	Tp	To	Cc	Np	Ac	Ca
0.75	0	0	0	0	0	0
1.5	28	11	6	8	10	3
3	35	16	9	31	15	5
6	42	20	22	27	23	17
12	45	33	27	19	29	33
18	43	50	36	33	31	35
24	35	36	42	47	46	54
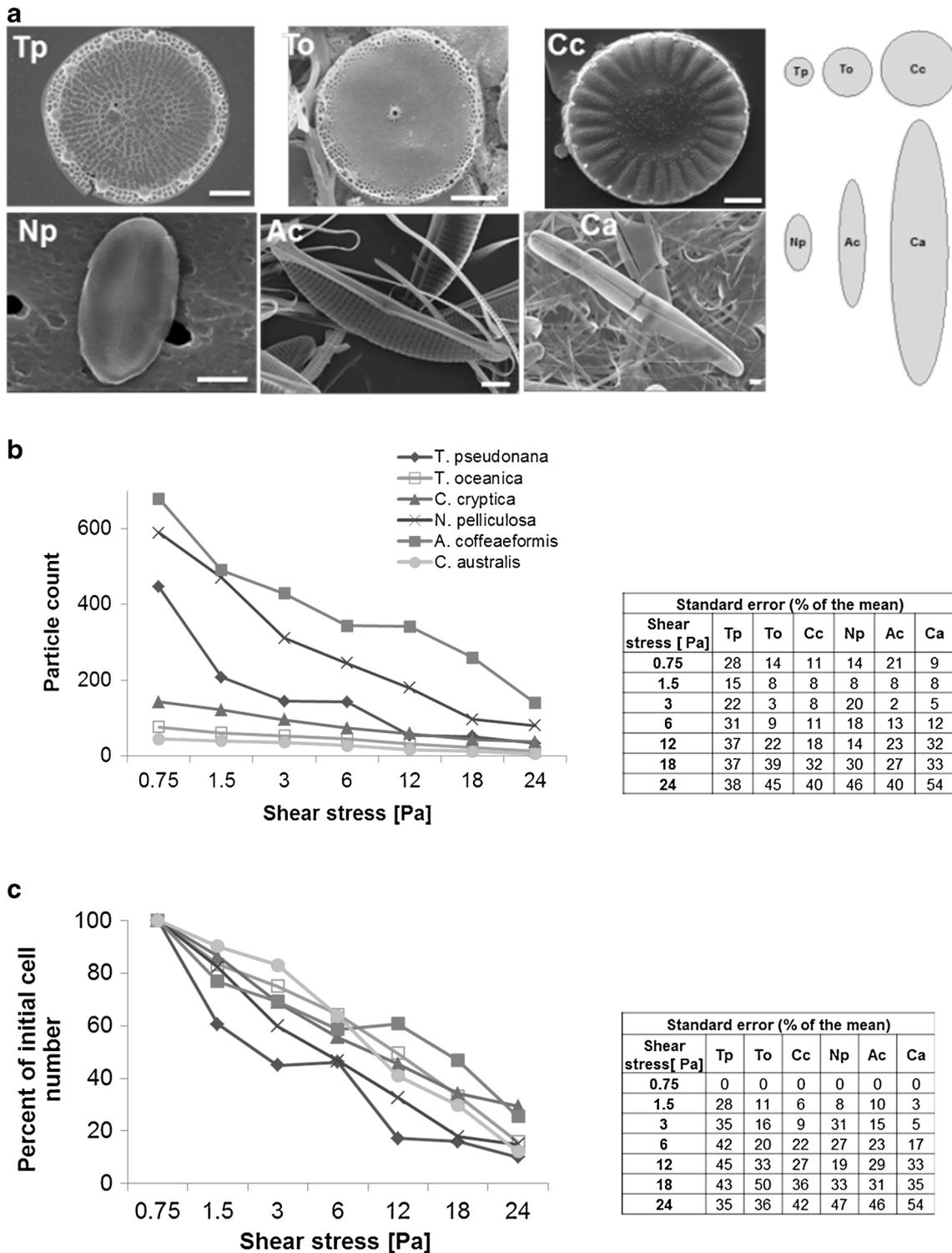
Fig. 5 **a** SEM images of silica valve structures from diatom species chosen for comparison of adhesive properties, and a schematic of their relative size and geometric representation. Centric diatoms: Tp- *Thalassiosira pseudonana*; To- *Thalassiosira oceanica*; Cc- *Cyclotella cryptica*. Pennate diatoms: Np- *Navicula pelliculosa*; Ac- *Amphora coffeaeformis*; Ca- *Craspedostauros australis*. The scale bar is 2 μm.

b, **c** The retention of silica structures from selected species on glass slides after incremental increases in shear stress shown as: **b** number of cells remaining after each applied pressure; **c** percentage of initially adhered cells. For clarity, standard error values are shown in the tables to the right of graphs as a percent of the mean from four independent experiments
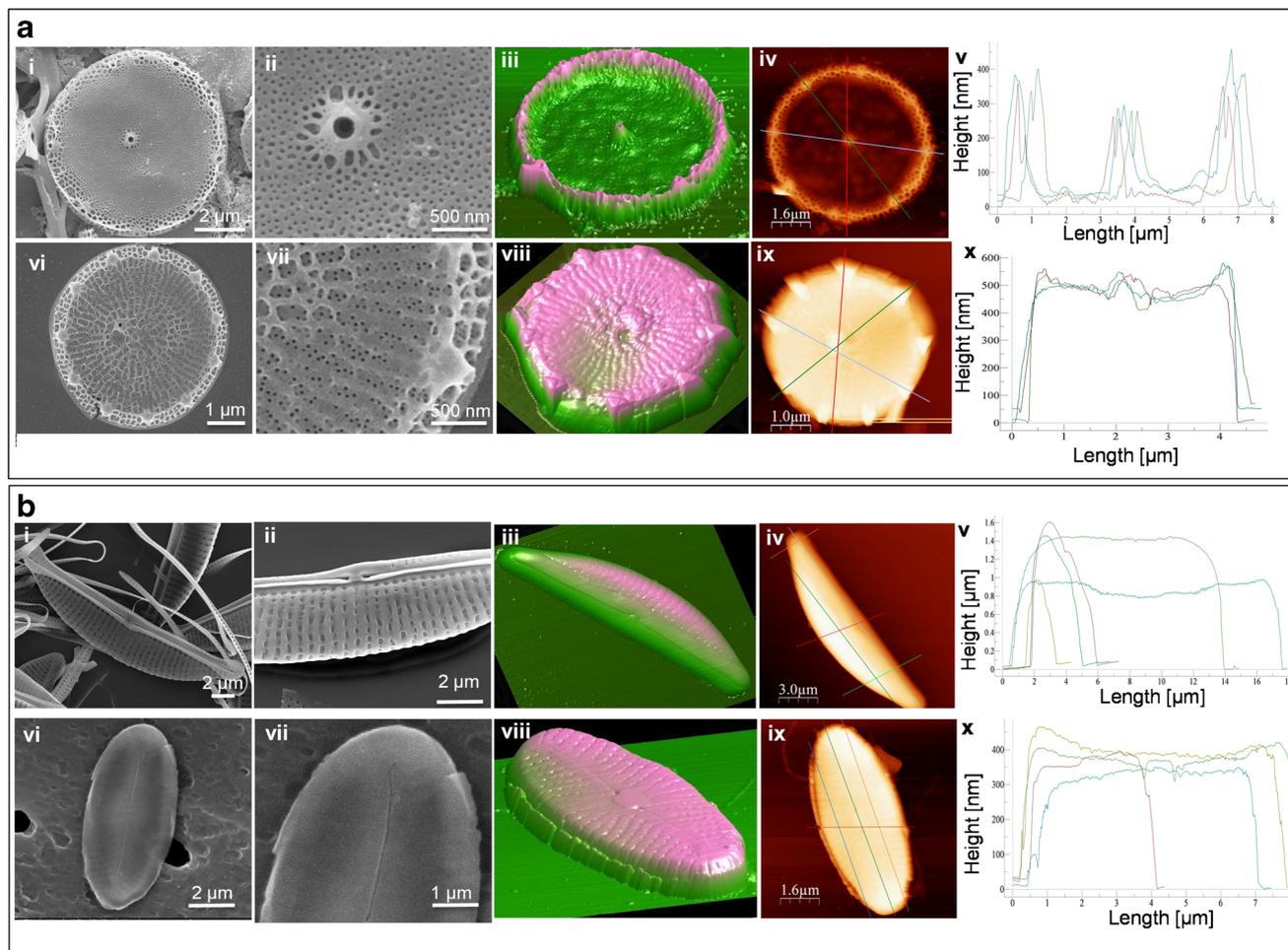
Fig. 6 Morphology comparison and possible surface contact area of: **a** centric diatoms *T. oceanica* (i–v) and *T. pseudonana* (vi–x); and **b** *A. coffeaeformis* (i–v) and *N. pelliculosa* (vi–x). SEM images of: the outer surface of the silica valve (i, vi) and magnification of the valve showing mesoscale texture (ii, vii). AFM images of valves in height mode in: 3D (iii, viii) and 2D (iv, ix) showing in pink predicted the silica-surface contact area. v and x show the profiles of the valves, colors indicate the profile on iv and ix

40], as described by the DLVO-theory [42]. As particles settle to the substrate, they first encounter the electrostatic double-layer repulsion, but some fraction of the particles overcome the potential barrier and come into close contact with the substrate. At this point, the attractive VDW and hydrogen bonding interactions create adhesion [26, 43]. A similar process governs particle-particle interactions.

The settling time experiment demonstrated that 16 hours was enough time to achieve maximum adherence (Fig. 3). The time of sedimentation driven by gravitational forces is dependent on the size and shape of a particle. For example a 10 μm particle needs approximately 2 h to sediment through 1 m of water [44]. Our experiment required longer settling times, indicating that in addition to sedimentation dynamics, the interaction of particles with each other and the substrate is significant. Double layer repulsion, as well as viscous drag of the hydration water layers on the

particles, can be expected to slow down the attachment process. Our observations were consistent with those of Yiantsios et al. [43], who found that the adhesion of particles (glass spheres) is dependent on settling time as a result of the particles having to overcome the electrostatic repulsion force that resists their approach to the surface.

Particles tend to adhere better to surfaces with similar wettability. Consistent with the hydrophilic nature of acid-cleaned diatom silica, adhesion was enhanced on increasingly hydrophilic surfaces (Fig. 4). The hydrophobic SAM-coated glass substrates would have reduced –OH content and would not be able to carry as much charge, leading to significant reductions in particle-surface electrostatic repulsion. Although increasingly hydrophobic substrates have less double-layer repulsion, they also have a reduced capacity to hydrogen bond with water or surface silanols on the silica particles. Consequently, adhesion, which depends

Shear stress [Pa]	Control	3	12	24
Mean length [μm]	14.31	14.50	14.51	15.67
St. Error	0.03	0.04	0.09	0.04
Mean width [μm]	4.95	5.03	5.04	5.58
St. Error	0.02	0.02	0.04	0.02
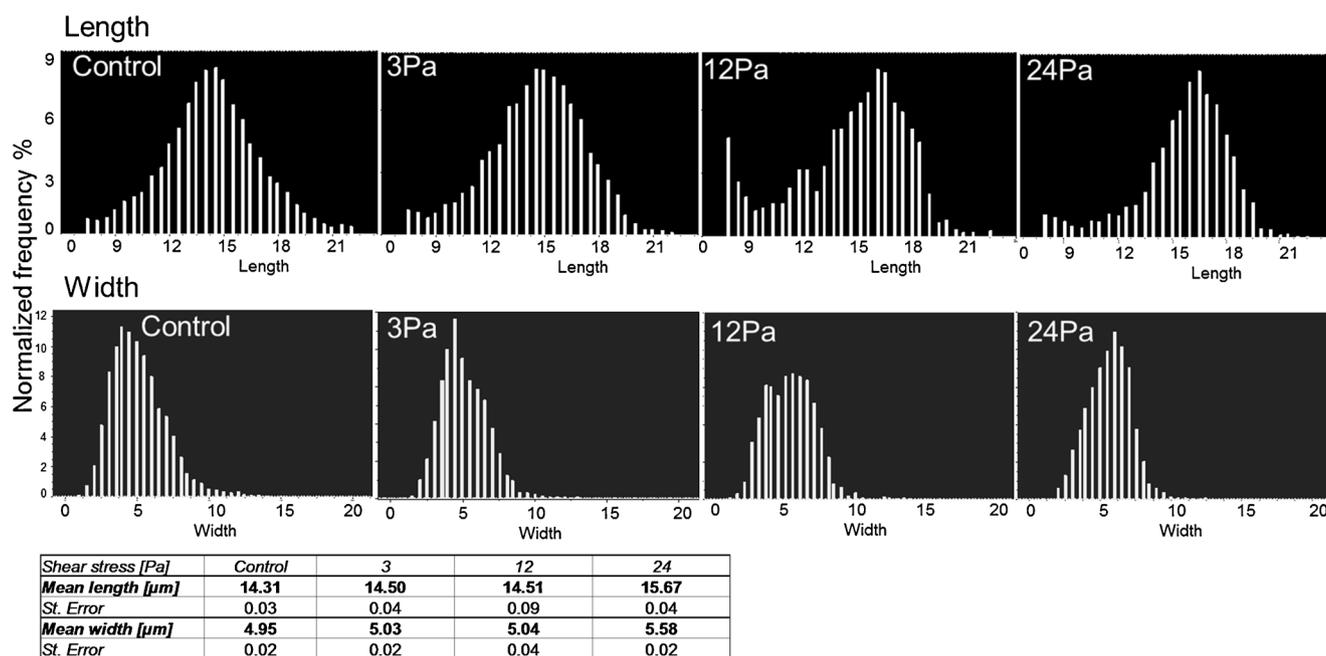
Fig. 7 Differences in length (*upper panels*) and width (*lower panels*) of *A. coffeaeformis* silica particles in the control sample and the eluent collected from the slide exposed to increasing shear force (3–24 Pa)

on the formation of short-range attractive contacts, is significantly reduced on hydrophobic surfaces. It should be kept in mind that the process of adhesion of acid-cleaned diatom silica is distinct from that of living diatoms. Living diatoms adhere better to hydrophobic substrates [5, 45–49], which is driven by the hydrophobic nature of the adhesive mucilage.

The comparison of acid-cleaned silica from six different species revealed two stages of adhesion, namely initial and persistent. As shown on Fig. S3 the preferable contact area for persistent adhesion is the outside of the valve, thus, these features are likely to contribute more substantially to adhesive properties. Initial adhesion appears to be dependent on surface contact area and particle size. Comparison of the two centric species with similar overall dimensions showed that *T. pseudonana* had a much larger area that could contact the substrate than *T. oceanica* (Fig. 6a).

Previous studies examining the adhesive characteristics of synthetic particles have been conducted on particles with simple, defined shapes; however, diatom silica has unique and complex features making it impractical to extrapolate from data acquired with synthetic particles. Accordingly, our investigation of acid-cleaned diatom silica yielded an unanticipated result. Mullins et al. (1992) showed under dry conditions that adhesion of particles with simple geometric shapes decreases in order for plates, cylinders, and spheres of a given mass [49]. We found that *A. coffeaeformis* adhered better than *N. pelliculosa*, which apparently contradicts the documented better adhesion of plate-like (i.e.

N. pelliculosa) structures [46]. We propose, however, that the curved shape of *A. coffeaeformis* enables more contact possibilities under high particle densities than the planar *N. pelliculosa*, which would have to land flat on the surface to have a high proportion contact area. In spite of the curved nature of *A. coffeaeformis'* structure, close analysis reveals one major area with very gentle curvature that could serve as a contact surface, another face containing the raphe (the contact surface in living cells) that is quite flat, and a smaller flat face which if landed on, would tend to reorient the valve to lie on the raphe face (Fig. 8). Further, the hydrodynamic shape of *A. coffeaeformis* may explain its increased adherence at a higher shear forces than the other species (Fig. 5c).

Differences between species in persistent adhesion were less substantial than in initial adhesion. We expect the chemistry of the silica surfaces to be similar between species [8, 9]. Short-range attractive forces will contribute to adhesive contacts as discussed above. Once initially non-adherent particles are removed in the 0.75 Pa wash, the remaining adherent particles for each species appear to have sufficient contact area such that any morphology-induced differences in contact area are difficult to detect. Secondly, the hydrodynamic forces exerted on adherent particles will vary in a complex manner with morphology [39, 50]. Most studies of particle detachment under hydrodynamic flow have examined spherical or rod-like particles, and have shown that contributions from tangential shear forces can lead to particle sliding, moment forces induced on the particles can
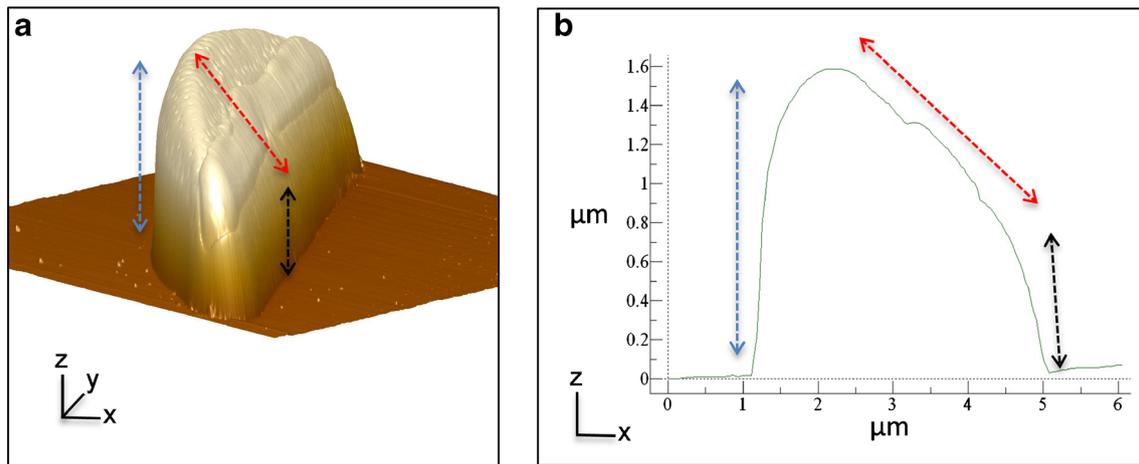
Fig. 8 Morphology of *A. coffeaeformis*. **a** AFM image of the valve from Fig. 6b iv rotated to highlight surface features. *Red line* indicates the flat surface of the raphe face. *Blue line* shows the flat surface in the z-plane, however this surface displays a gently curving convex shape in the y-plane. The *black line* shows another flat surface on the short edge of the valve. **b** Valve profile with *arrows* corresponding to arrows in (**a**) for reference. Coordinates are indicated in the figure

lead to rolling, and lift forces can lead to detachment in the normal direction. Studies have indicated the importance of the rolling detachment mechanism [50]. However, the surface roughness on both the particle and the substrate seems to play a principal role in determining detachment strength. The glass substrates should have uniform roughness, but the various diatom species with differing mesotopography can play a significant role in determining detachment mechanism and strength. The modeling of all of these combined effects for the wide variety of shapes explored here is beyond the scope and aim of this study. It is likely that subtle changes in shape and mesotopography of the silica particles lead to complex interactions between hydrodynamic forces applied, and some of these may even cancel one another. This expected complexity probably explains the more subtle dependence of detachment on morphology in the persistent stage of adhesion.

In terms of the effect of size, we show that larger particles of *A. coffeaeformis* persisted under higher shear stresses (Fig. 7). This could be due to increased surface contact area. However, the largest species tested, *C. australis*, adhered very poorly. It can be best compared in overall shape to *N. pelliculosa*, but has a much higher aspect ratio (7:1 vs. 1.7:1). The higher aspect ratio and size apparently leads to larger effective hydrodynamic forces being imparted to these particles during flow, resulting in more detachment.

5 Conclusions

Previous work has characterized the adhesive properties of silica particles with well-defined shapes. Our analysis was aimed at evaluating the adhesion of diatom silica, which has

complex shapes at different scales, and which is difficult to model as a surface. To accomplish this, we adapted the PFC approach, which allowed experimental comparison of adhesive properties. This investigation of diatom silica adhesion examined features such as initial and persistent adhesion, dry and wet environments, substrate properties and compared different silica mesomorphologies. We established similarities in adhesive properties between model silica particles and diatoms, but the diatoms generally adhered much better, indicating a contribution by their morphology. There was a correlation between surface area relative to size and the initial adhesion, but results obtained with *A. coffeaeformis* also suggested that a greater probability of surface contact based on shape was a factor. Our data suggests that *A. coffeaeformis* has an optimal combination of shape and size enabling strong initial and persistent adhesion. Identification of this shape based on models developed on defined silica particles would not have been likely.

References

1. Chiovitti A, Dugdale T, Wetherbee R (2006) Diatom adhesives: molecular and mechanical properties. In: Smith A, Callow J (eds) Biological adhesives. Springer Berlin Heidelberg, pp 79–103
2. Wetherbee R, Lind JL, Burke J, Quatrano RS (1998) Minireview-the first kiss: establishment and control of initial adhesion by raphid diatoms. J Phycol 34:9–15

3. Molino PJ, Wetherbee R (2008) The biology of biofouling diatoms and their role in the development of microbial slimes. Biofouling 24:365–379

4. Molino PJ, Hodson OM, Quinn JF, Wetherbee R (2006) Utilizing QCM-D to characterize the adhesive mucilage secreted by two marine diatom species *in-situ* and in real-time. Biomacromolecules 7:3276–3282

5. Holland R, Dugdale TM, Wetherbee R, Brennan AB, Finlay JA, Callow JA, Callow ME (2004) Adhesion and motility of fouling diatoms on a silicone elastomer. Biofouling 20:323–329

6. Schultz M, Finlay J, Callow M, Callow J (2000) A turbulent channel flow apparatus for the determination of the adhesion strength of microfouling organisms. Biofouling 15:243–251

7. Higgins MJ, Molino P, Mulvaney P, Wetherbee R (2003) The structure and nanomechanical properties of the adhesive mucilage that mediated diatom-substratum adhesion and motility. J Phycol 39:1181–1193

8. Tesson B, Hildebrand M (2013) Characterization and localization of insoluble organic matrices associated with diatom cell walls: insight into their roles during cell wall formation. PloS One 8(4):e61675

9. Dixit S, Van Cappellen P (2002) Surface chemistry and reactivity of biogenic silica. Geochimica et Cosmochimica Acta 66(14):2559–2568

10. Kröger N, Poulsen N (2008) Diatoms-from cell wall biogenesis to nanotechnology. Annu Rev Genet 42:83–107

11. Gordon R, Losic D, Tiffany MA, Nagy SS, Sterrenburg FAS (2009) The Glass Menagerie: diatoms for novel applications in nanotechnology. Trends Biotechnol 27:116–127

12. Ehrlich H (2010) Hierarchical biological materials. Biol Mater Mar Orig 125–136

13. Losic D, Mitchell JG, Voelcker NH (2009) Diatomaceous lessons in nanotechnology and advanced materials. Adv Mater 21:2947–2958

14. Hildebrand M (2005) Prospects of manipulating diatom silica nanostructure. J Nanosci Nanotechnol 5:146–157

15. Aw MS, Simovic S, Yu Y, Addai-Mensah J, Losic D (2012) Porous silica microshells from diatoms as biocarrier for drug delivery applications. Powder Technol 223:52–58

16. Bismuto A, Setaro A, Maddalena P, Destefano L, Destefano M (2008) Marine diatoms as optical chemical sensors: a time-resolved study. Sensors Actuators B Chem 130:396–399

17. Yamanaka S, Yano R, Usami H, Hayashida N, Ohguchi M, Takeda H, Yoshino K (2008) Optical properties of diatom silica frustule with special reference to blue light. J Appl Phys 103:074701–074701

18. Fuhrmann T, Landwehr S, El Rharbi-Kucki M, Sumper M (2004) Diatoms as living photonic crystals. Appl Phys B Lasers Opt 78:257–260

19. Lee S-J, Huang C-H, Shian S, Sandhage KH (2007) Rapid hydrolysis of organophosphorous esters induced by nanostructured, fluorine-doped titania replicas of diatom frustules. J Am Ceramic Soc 90:1632–1636

20. Sandhage KH, Dickerson MB, Huseman PM, Caranna MA, Clifton JD, Bull TA, Heibel TJ, Overton WR, Schoenwaelder MEA (2002) Novel, bioclastic route to self-assembled, 3D, chemically tailored meso/nanostructures: shape-preserving reactive conversion of biosilica (diatom) microshells. Adv Mater 14:429–433

21. Mann DG, Droop SJM (1996) Biodiversity, biogeography and conservation of diatoms. Hydrobiologia 336:19–32

22. Davis AK, Hildebrand M (2008) Molecular processes of biosilicification in diatoms. Met Ions Life Sci Biomineralization Nat Appl 4:255–294

23. Hasle GR, Syvertsen EE, Steidinger KA, Tangen K, Tomas CR (1996) Identifying marine diatoms and dinoflagellates. Academic, p 598

24. Tesson B, Hildebrand M (2010) Extensive and intimate association of the cytoskeleton with forming silica in diatoms: control over patterning on the meso- and micro-scale. PloS One 5:e14300

25. Round FE, Crawford RM, Mann DG (1990) Diatoms: biology and morphology of the genera. Cambridge University Press, Cambridge, p 758

26. Corn M (1961) The adhesion of solid particles to solid surfaces II. J Air Pollut Control Assoc 11(12):566–584

27. Hodson OM, Monty JP, Molino PJ, Wetherbee R (2012) Novel whole cell adhesion assays of three isolates of the fouling diatom Amphora coffeaeformis reveal diverse responses to surfaces of different wettability. Biofouling: J Bioadhesion Biofilm Res 28:381–393

28. Reimann BEF, Leivin JC, Volcani BE (1966) Studies on the biochemistry and fine structure of silica shell formation in diatoms. II. The structure of the cell wall of Navicula pelliculosa Bréb. J Phycol 2:74–84

29. Darley WM, Volcani BE (1969) Role of silicon in diatom metabolism. Exp Cell Res 58:334–342

30. Hildebrand M, Holton G, Joy DC, Doktycz MJ, Allison DP (2009) Diverse and conserved nano- and mesoscale structures of diatom silica revealed by atomic force microscopy. J Microsc 235:172–187

31. Horcas I, Fernández R, Gómez-Rodríguez JM, Colchero J, Gómez-Herrero J, Baro AM (2007) WSXM: a software for scanning probe microscopy and a tool for nanotechnology. Rev Sci Instrum 78:013705

32. Callow ME, Callow J, Ista LK, Coleman SE, Nolasco AC, López GP (2000) Use of self-assembled monolayers of different wettabilities to study surface selection and primary adhesion processes of green algal (Enteromorpha) zoospores. Appl Environ Microbiol 66(8):3249–3254

33. Van Blaaderen A, Vrij A, Blaaderen AV (1992) Synthesis and characterization of colloidal dispersions of fluorescent, monodisperse silica spheres. Langmuir 81:2921–2931

34. Desclés J, Vartanian M, El Harrak A, Quinet M, Bremond N, Sapriel G, Bibette J, Lopez PJ (2008) New tools for labeling silica in living diatoms. New Phytol 177:822–829

35. Won D, Zhu S-N, Chen M, Teichert A-M, Fish JE, Matouk CC, Bonert M, Ojha M, Marsden PA, Cybulsky MI (2007) Relative reduction of endothelial nitric-oxide synthase expression and transcription in atherosclerosis-prone regions of the mouse aorta and in an in vitro model of disturbed flow. Am J Pathol 171:1691–1704

36. Muro S, Dziubla T, Qiu W, Leferovich J, Cui X, Berk E, Muzykantov VR (2006) Endothelial targeting of high-affinity multivalent polymer nanocarriers directed to intercellular adhesion molecule 1. J Pharmacol Exp Ther 317:1161–1169

37. Sharma MM, Chamoun H, Sarma D, Schechter RS (1992) Factors controlling the hydrodynamic detachment of particles from surfaces. J Colloid Interface Sci 149(1):121–134

38. Lin H, Gomez I, Meredith JC (2013) Pollenkitt wetting mechanism enables species-specific tunable pollen adhesion. Langmuir 29(9):3012–3023

39. Bowling RA (1985) An analysis of particle adhesion on semiconductor surfaces. J Electrochem Soc 132:2208

40. Visser J (1995) Particle adhesion and removal: a review. Part Sci Technol 37–41

41. Kim J, Lawler D (2005) Characteristics of zeta potential distribution in silica particles. Bull-Korean Chem Soc 7:1083–1089

42. Verwey EJW, Overbeek JTG (1999) Theory of the stability of lyophobic colloids. Courier Dover Publications, p 205

43. Yiantsios SG, Karabelas AJ (1995) Detachment of spherical microparticles adhering on flat surfaces by hydrodynamic forces. J Colloid Interface Sci 176:74–85

44. Koohestanian A, Hosseini M, Abbasian Z (2008) The separation method for removing of colloidal particles from raw water. Euras J Agric Environ Sci 4:266–273

45. Finlay JA, Callow ME, Ista LK, Lopez GP, Callow JA (2002) The influence of surface wettability on the adhesion strength of settled spores of the green alga enteromorpha and the diatom amphora. Integr Comp Biol 42:1116–1122

46. Wang Y, Pitet LM, Finlay JA, Brewer LH, Cone G, Betts DE, Callow ME, Callow JA, Wendt DE, Hillmyer MA, DeSimonea JM (2011) Investigation of the role of hydrophilic chain length in amphiphilic perfluoropolyether/poly(ethylene glycol) networks: towards high-performance antifouling coatings. Biofouling 27:1139–1150

47. Sundaram HS, Cho Y, Dimitriou MD, Weinman CJ, Finlay JA, Cone G, Callow ME, Callow JA, Kramer EJ, Ober CK (2011) Fluorine-free mixed amphiphilic polymers based on PDMS and PEG side chains for fouling release applications. Biofouling 27:589–602

48. Schilp S, Kueller A, Rosenhahn A, Grunze M, Pettitt ME, Callow ME, Callow JA (2007) Settlement and adhesion of algal cells to hexa(ethylene glycol)-containing self-assembled monolayers with systematically changed wetting properties. Biointerphases 2:143–150

49. Mullins M, Michaels L, Menon V, Locke B, Ranade M (1992) Effect of geometry on particle adhesion. Aerosol Sci Technol 17(2):105–118

50. Lameiras FS, Souza ALD, Melo VRARD, Nunes EHM, Braga ID (2008) Measurement of the zeta potential of planar surfaces with a rotating disk. Mater Res 11(2):217–219